Journal of Cleaner Production 187 (2018) 250–256

Contents lists available at ScienceDirect

Journal of Cleaner Production

journal homepage: www.elsevier.com/locate/jclepro

Functional glass-ceramic foams from 'inorganic gel casting' and sintering of glass/slag mixtures

Acacio Rincón, Daniele Desideri, Enrico Bernardo*

Dipartimento di Ingegneria Industriale, University of Padova, Italy

ARTICLE INFO

Article history:
Available online 20 March 2018

Keywords:
Gel casting
Alkali activation
Glass ceramic foams
Copper slag
Electromagnetic shielding

ABSTRACT

The here described investigation was essentially aimed at exploring the chemical stabilization and reutilization of iron-rich slag from copper metallurgy, by the manufacturing of glass-ceramic foams. The foams were developed according to a new method, recently reported for pure recycled soda-lime glass. Mixtures of soda-lime glass/slag powders (with slag content ranging from 10 to 30 wt%), suspended in alkaline aqueous solution, underwent progressive low temperature (80 °C) hardening, owing to the formation of hydrated calcium silicate compounds (C–S–H). Before complete setting, an extensive foaming could be achieved by vigorous mechanical stirring, with the help of a surfactant.

After foaming, glass/slag mixtures could be sintered at 800–1000 °C; the mutual interaction caused an extensive crystallization, with precipitation of Ca–Fe silicates and iron oxides (hematite and magnetite), promoting the mechanical properties (up to 4.4 MPa, with a porosity of about 80%). Leaching test confirmed the stabilization of pollutants, from the slag, in the final ceramics. Owing to the separation of iron oxides, particularly magnetite, the newly obtained foams exhibited a ferrimagnetic behavior, that could be exploited in electromagnetic shielding applications.

1. Introduction

In world copper production, about 30 million tonnes of copper slag are produced annually, considering that 2.2–3 tons of slag are generated for each ton of metal obtained (Gorai and Jana, 2003). The heavy metals included in the slag could be leached away and dispersed in the environment, if a proper disposal or stabilization treatment is not applied.

Contaminations represent a fundamental issue for the reuse of copper slag - known also as 'fayalite slag' (owing to the presence of a specific iron silicate, $FeSiO_3$) - in any high value new material (Lottermoser, 2002; Van der Sloot and Dijkstra, 2004). As an example, the slag can be reused only in limited quantity, as pozzolanic material, due to the potential leaching of heavy metals (Zain et al., 2004). It may be used, in concrete, as coarse aggregate (Moura et al., 2007; Al-Jabri et al., 2009; Najimi et al., 2011) or, outside building industry, as low cost abrasive (Kambham et al., 2007).

A recently proposed approach, for the upcycling of copper slag in building applications, is represented by 'geopolymer-like' inorganic polymers, approaching conventional Portland concrete in terms of strength and durability (Mithun and Narasimhan, 2016), but generally featuring a smaller CO_2 footprint (Provis et al., 2009; Peys et al., 2017). The literature evidences a strong dependence between the characteristics of the activating solution and the formation of a truly geopolymeric (zeolite-like) network. A proper reactivity, in fact, is achieved with sodium hydroxide solutions (possibly replaced by sodium silicate) at high molarity (Onisei et al., 2015). Other studies prove the evolution of the geopolymeric reaction, producing geopolymer mortars from fayalitic slag, by increasing temperature and curing times (Nazer et al., 2016).

Few studies were actually performed taking into account the possible leaching of heavy metals from inorganic polymers made from fayalitic slag. It was established that the curing conditions play a direct effect on the mechanical properties, but do not exhibit a direct influence on the leachability (Iacobescu et al., 2017): even if the geopolymer matrix presents a good immobilization of most of heavy metals, the leaching of Cr ions is still possible.

The investigation reported here was essentially aimed at offering a strategy that could combine the stabilization of copper slag with its reutilization in the manufacturing of highly porous glass-ceramic foams, to be used in the building industry, as thermal

* Corresponding author.
E-mail address: enrico.bernardo@unipd.it (E. Bernardo).

https://doi.org/10.1016/j.jclepro.2018.03.065

and acoustic insulators. In general, glass-ceramics represent the most established valorization way for inorganic waste, supported by a vast literature (Rawlings et al., 2006; Chinnam et al., 2013; Rincón et al., 2016) but we must observe that the melting of waste ('vitrification') and the subsequent thermal treatment for the transformation of glasses into partially crystallized products imply extra costs. The situation is even more complicated for cellular materials, in which the gas evolution, from selected additives, should be carefully coupled with viscous flow sintering and crystallization (Rincón et al., 2016).

The approach adopted in the research reported here actually combined several strategies for energy saving. First, glass-ceramics were obtained by direct sintering of recycled glass and slag. The direct treatment relies on the formation of silicate and aluminosilicate crystals, similar to those produced by crystallization of waste glasses, by interaction of recycled glasses with inorganic waste, upon heat treatment. This fact supports the use of the term 'glass-ceramic', despite the absence of any melting step (Chinnam et al., 2013; Rincón et al., 2016). Second, a cellular structure was developed according to recent experiences on the low temperature foaming of geopolymers, by intensive mechanical stirring of alkali activated suspensions (with the help of a surfactant) (Cilla et al., 2014), although at much weaker alkali concentrations and far from the conditions for the development of inorganic polymers.

Operating with soda-lime glass, the hardening corresponds to the development of calcium silicate hydrates (C–S–H type) at the surfaces of particles, later subjected to viscous flow sintering upon firing (Rincón et al., 2017). Since a cellular structure is already available, there is no need for any foaming agent (e.g. C or SiC) and the sintering temperature is moderate (700 °C, instead of 850–950 °C required for activating the foaming agents) (Scarinci et al., 2005).

Mixing soda-lime glass with copper slag makes determined the need for higher sintering temperatures (at least 800 °C), in turn leading to complex glass-slag interactions. These interactions were based on the oxidative decomposition of fayalite, and led to a significant crystallization of the foamed products, with precipitation of iron oxides. Despite a homogeneous glass matrix was not achieved, the glass-ceramic products exhibited the desired stabilization of heavy metals, essential for the application of foams in thermal and acoustic insulation. In selected conditions, the precipitation of iron oxides led to a ferri-magnetic behaviour, configuring 'multifunctional' porous glass-ceramics.

2. Materials and methods

Both starting materials consisted of waste. Iron rich slag coming from copper metallurgy, later referred to 'CS' was provided by KU Leuven (Belgium), with a mean particle size of 45 μm. Soda lime glass ('SLG') was provided by SASIL SpA (Biella, Italy), in the form of fine powders (mean particle size of 75 μm). The latter corresponds to the finely powdered glass fraction of the municipal solid waste collection that remains practically unusable after colour selection, due to the presence of polymer, ceramic and metallic contaminations that prevents its use in the manufacturing of new glass containers. The chemical composition of the two starting waste materials, from previous investigations (Ponsot et al., 2014), is shown in Table 1.

Fine powders of SLG and CS, in a proportion 80/20 and 70/30 wt % were mixed in an aqueous solution containing 2.5 M KOH (reagent grade, Sigma– Aldrich, Gillingham, UK), to a final solid loading of 65 wt%. The powders were subjected to alkaline attack for 3 h, under low speed mechanical stirring (500 rpm; ArgoLab AM 20-D mixer, Test Srl, Perugia, Italy). After alkaline activation, the obtained suspensions were cast in closed polystyrene cylindrical moulds (60 mm diameter), and cured at 75 °C, for 2 h. After addition of a non-ionic surfactant Triton X-100 (Sigma-Aldrich, Gillingham, UK), for an amount of 4 wt%, partially hardened suspensions were foamed by vigorous mechanical mixing (2000 rpm; same mixer used above). Foamed 'green' foams were kept in the same moulds at 40 °C for 24 h, in order to complete the curing, and then demoulded. Finally, 60 mm diameter hardened 'green' foams were fired at temperatures between 800 and 1000 °C, for 1 h, with a heating rate of 10 °C/min.

Table 1
Chemical composition (expressed in wt.%) of the starting materials.

Oxide (wt%)	SiO_2	FeO	Al_2O_3	Na_2O	K_2O	MgO	CaO	ZnO
CS	29	52	4	<1	<1	1	2	7
SLG	71.6	–	1	13.5	0.4	3.9	9	–

Selected samples were subjected to thermogravimetric analysis (TGA, STA409, Netzsch Gerätebau GmbH, Selb, Germany) operated at 10 °C/min in static air from room temperature up to 1000 °C. Fourier-transform infrared spectroscopy (FTIR, FTIR model 2000, Perkin Elmer Waltham, MA) was conducted in pellets prepared by mixing ≈1 wt% of the finely powdered sample with KBr powder operating in absorbance mode with a 4 cm^{-1} resolution for 32 scans in the 4500–400 cm^{-1} region.

The morphological and microstructural characterizations were performed by optical stereomicroscopy (AxioCam ERc 5s Microscope Camera, Carl Zeiss Microscopy, Thornwood, New York, US) and scanning electron microscopy (FEI Quanta 200 ESEM, Eindhoven, The Netherlands). The mineralogical analysis was conducted by X-Ray Diffraction analysis (XRD) on powdered samples (Bruker D8 Advance, Karlsruhe, Germany – CuKα radiation, 0.15418 nm, 40 kV–40 mA, $2\theta = 10–70°$, step size 0.05°, 2 s counting time). The phase Identification was performed by means of the Match!® program package (Crystal Impact GbR, Bonn, Germany), supported by data from PDF-2 database (ICDD-International Centre for Diffraction Data, Newtown Square, PA).

The geometric density (ρ_g) of fired foams was evaluated by considering the mass to volume ratio. The apparent (ρ_a) and the true density (ρ_t) were measured by using a helium pycnometer (Micromeritics AccuPyc 1330, Norcross, GA), operating on bulk or on finely crushed samples, respectively. The three density values (ρ_g, ρ_a, and ρ_t) were used to compute the amounts of open and closed porosity (Martin-Marquez et al., 2008). The obtained foams were subjected to compression tests by using an Instron 1121 UTS (Instron, Danvers, MA) machine, with a crosshead speed of 1 mm/min, employing samples of about 10 mm × 10 mm × 10 mm, cut from larger specimens (each data point corresponding to 10–12 samples).

Electromagnetic shielding effectiveness was measurement with a coaxial waveguide, originally developed for thin films, and already proven to be appropriate for porous ceramics (Maschio et al., 2016). Measures were taken in the range form 0–3 GHz.

The release of heavy metals was evaluated by application of a leaching procedure according to European Standard for waste toxicity evaluation (EN 12457-2). Fragments below 4 mm were placed in an extraction solution consisting of distilled water, with a pH value of ~7, for a liquid/solid ratio of 10, and softly stirred at 25 °C for 24 h. The resulting solutions were filtered through a 0.6 μm filter and analysed using inductively coupled plasma (ICP; SPECTRO Analytical instruments GmbH, Kleve, Germany).

3. Results and discussion

The nature of the hydrated compounds, formed after the alkali

activation and subsequent curing of the hardened foams, and their transformation after the heat treatment could be studied by means of infrared spectroscopy and the TGA- DTA analysis. Fig.1 reports the FTIR spectra of SL glass and CS slag at the starting stage as well after alkali activation and thermal treatment at 900 °C of the 70/30 SL/CS mixture.

Soda lime glass cullet presented its typical absorption bands i.e. the Si–O–Si asymmetrical stretching at 1050 cm^{-1} and the bending mode between 700 and 800 cm^{-1}. The band at 450 cm^{-1} could be assigned to the Si–O–Si rocking mode (Dussauze et al., 2010; Attila et al., 2013), CS presented the characteristics bands of fayalite slags with bands at 955, 910 and 877 cm^{-1}, corresponding to the asymmetric stretching vibrations of SiO_4, and at 828 cm^{-1}, corresponding to the symmetric stretch (Onisei et al., 2015). The bands appearing between 600 and 400 cm^{-1} correspond to rotations of the SiO_4 and transitions of the iron cations in the structure (Lane et al., 2011).

A quite wide absorption band appeared for the hardened 'green' foam between 3000 and 3700 cm^{-1}. It could be assigned to stretching vibration of O–H groups, as a consequence of hydration processes. While the weak signals in CS and SLG could be attributed to atmospheric hydration, the band in the hardened foam was related to formation of C–S–H products, after alkali activation. A band centred at 2900 cm^{-1}, assigned to C–H vibrations of the organic surfactant, was also detected only for hardened foams.

After the firing treatment the band assigned to the C–S–H was no longer present, as a result of thermal decomposition of the hydrated compound. The other bands present in the hardened and fired foams, in the range 1000–850 cm^{-1}, were attributed to Si–O asymmetric stretching vibrations. In the range 450–500 cm^{-1}, vibrations associated to (O–Si–O) deformation could be finally observed.

Fig.2a shows the thermogravimetric plot of surfactant (normalized according to the actual content of 4 wt%) and hardened glass-slag mixtures. The weight losses around 2–3 wt%, below 200 °C, could be attributed to the loss of physically bonded water, consistent with the wide endothermic bands in the DTA plot (Fig.2b). The further slight weight losses, between 300 and 600 °C, could not be attributed simply to the surfactant burn-out. The specific plot for the additive, alone, demonstrates that the related weight loss was complete at 400–450 °C; moreover, the overall losses were higher (>6%) than the amount of surfactant added. After burn out of surfactant, a contribution to the total losses could be attributed to the evolution of physically bonded water again and to the dehydroxylation of the above-mentioned C–S–H compounds formed after the alkali activation (the latter contributing even above 600 °C, Haq et al., 2014). The difference among the mixtures is consistent with this attribution: higher losses in the mixture 80/20 sample were expected, as a consequence of the higher soda-lime glass content, leading to C–S–H (Tchakout et al., 2017). The slight weight increase from 800 to 1000 °C could be attributed to oxidation reactions, i.e. changes in the valence state of iron ions (Marangoni et al., 2016).

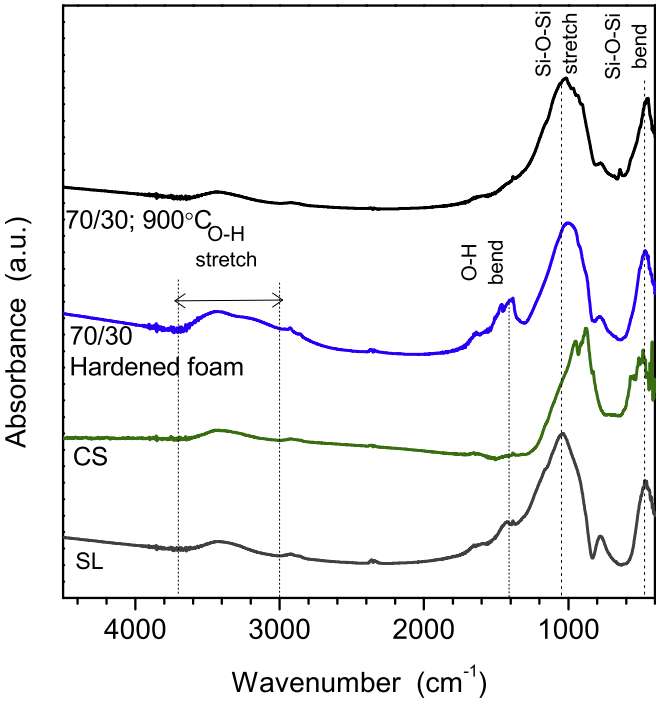

Fig. 1. FTIR spectra of selected materials.

Fig.3a and 3e illustrate the microstructure of 'green' foams (fracture surfaces, investigated by means of optical stereomicroscopy) for the mixtures SLG/CS 80/20 and 70/30, after 24 h of post-foaming curing, respectively. The other images show the microstructural changes after the heat treatment at 800, 900 and 1000 °C. The foams after activation and hardening feature a high microstructural uniformity, with most pores having a diameter around 100 μm for the 80/20 (80% SLG – 20% CS) mixture and 250 μm for the 70/30 (70% SLG – 30% CS) mixture. The difference in the pore size can be considered as a further effect of the 'dilution' of soda-lime glass operated by the slag. With a low soda-lime glass content, the reduced formation of C–S–H compounds reduced the viscosity of the starting suspension, causing some cell coalescence. On the contrary, in the 80/20 mixture the enhanced hardening led to the 'freezing' of a multitude of small pores.

The firing treatment had substantial effects on the microstructure. Our previous investigation on pure soda-lime glass (Rincón et al., 2017) [19] evidenced the occurrence of some pore reshaping, due to viscous flow; the cellular structure was not subjected to any coarsening, but the formation of thin membranes between adjacent pores transformed many open cells into closed cells. The reshaping in pure soda-lime glass was attributed to the decomposition of the hydrated phases upon hardening; this effect, due to the previously mentioned 'dilution', was reasonably reduced in glass/slag foams.

The observed significant pore reshaping upon firing could be due to glass/slag reactions, in the light of the instability of fayalite, from the slag, in oxidative atmosphere. Fayalite undergoes oxygenolysis according to the following reactions, forming hematite (Fe_2O_3) and magnetite (Fe_3O_4), respectively (Gyurov et al., 2014):

$$4\ FeO{\cdot}SiO_2 + O_2 \rightarrow 2\ Fe_2O_3 + 4\ SiO_2 \quad (1)$$

$$6\ FeO{\cdot}SiO_2 + O_2 \rightarrow 2\ Fe_3O_4 + 6\ SiO_2 \quad (2)$$

The by-product of slag oxygenolysis consists of amorphous silica, reasonably dissolved in softened soda-lime glass (Brinkmann and Laqua, 1985).

The oxidation could be a justification for the slight weight increase detected in the thermogravimetric plots of Fig.4a. However, it should be noted that thermal analysis does not represent effects that may arise upon time. In particular, it has been already shown that iron oxides, with increasing firing temperature, may transform from phases with ferric ions (Fe^{3+}, in Fe_2O_3) into phases with ferrous ions (both Fe^{2+} and Fe^{3+}, in Fe_3O_4=$FeO{\cdot}Fe_2O_3$; only Fe^{2+}, in FeO), with oxygen release, exploited for foamed materials (Ponsot and Bernado, 2013, 2014):

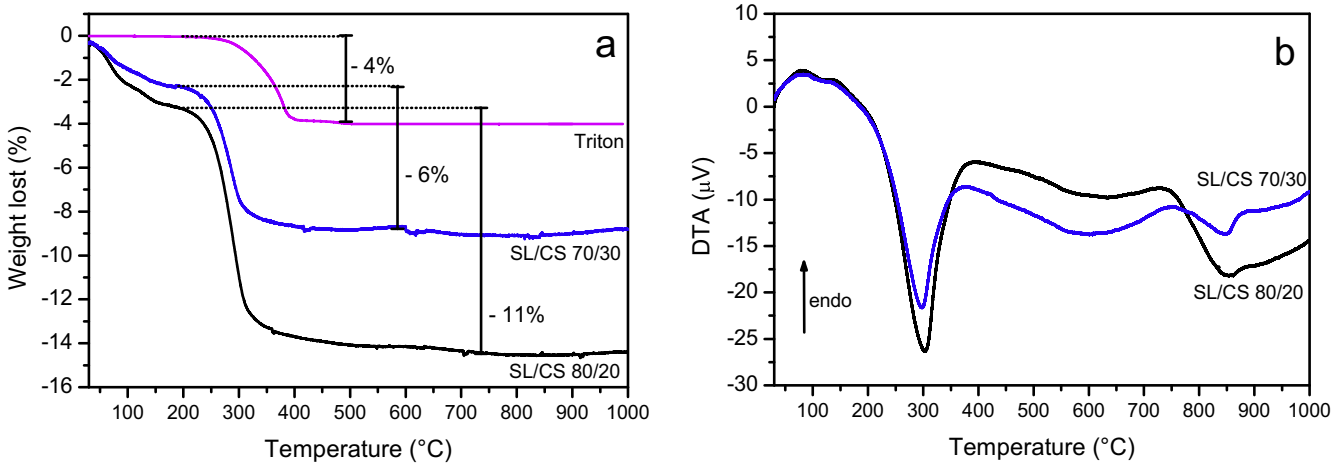

Fig. 2. Thermogravimetric (a) and DTA plots (b) of surfactant and hardened glass-slag mixtures.

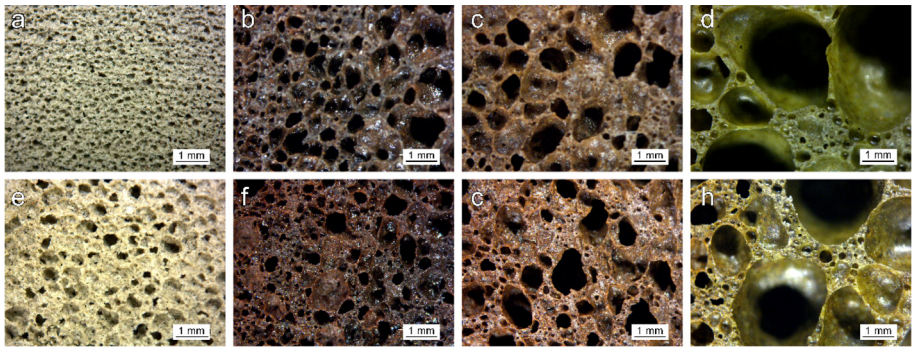

Fig. 3. Microstructural details of glass ceramic foams in the hardened state and after firing treatment: a–d) 80 SLG – 20 CS; e–h) 70 SLG – 30 CS; a, e) green state; b, f) 800 °C; c, g) 900 °C; d, h) 1000 °C.

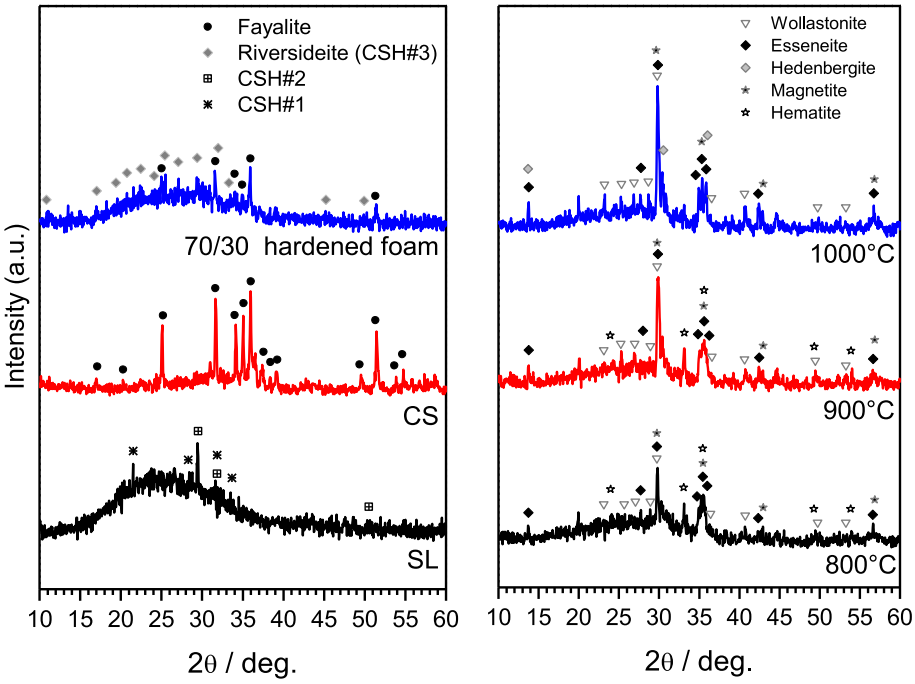

Fig. 4. X-ray diffraction patterns of glass foams (70% soda-lime glass-30% copper slag) in the hardened state (left) and after firing (right).

$$6\ Fe_2O_3 \rightarrow 4\ Fe_3O_4 + O_2 \quad (3)$$

$$2\ Fe_2O_3 \rightarrow 4\ FeO + O_2 \quad (4)$$

In other words, the thermal treatment likely determined a reaction chain, with an oxidation phase (decomposition of fayalite, known to start above 400 °C (Marangoni et al., 2016), possibly occurring during the heating step) followed by a reduction phase (release of oxygen, possibly occurring upon holding at the firing temperature).

The above described phenomenology was confirmed by the X-ray diffraction analysis. As described by Fig.4a, fayalite (Fe_2SiO_4, PDF#87-0317) remained after alkali activation of glass/slag mixture, in agreement with previous studies on inorganic polymers (Iacobescu et al., 2017; Pontikes et al., 2013). The amorphous halo, at the background, moved to higher 2θ values, compared to as received glass, in agreement with the compositional changes associated to the incorporation of network modifiers, caused by the same alkaline attack (Hemmings and Berry, 1987; Cyr et al., 2012). The starting glass actually featured some weak traces of calcium silicate hydrated phases (CSH#1, $Ca1.5SiO3.5 \cdot xH_2O$, PDF#33-0306; CSH#2, suolonite, $CaSiO_3 \cdot H_2O$, PDF#74-2248), likely due to surface reaction with environmental humidity; after mixing with fayalite slag and alkali activation, traces of another calcium silicate hydrated phase (CSH#3), attributable to a riversideite-type structure ($2CaSiO_3 \cdot 3H_2O$, PDF# 02-0600) were detected.

The firing treatments led to the precipitation of Ca–Fe silicates, with both Fe^{2+} and Fe^{3+} ions. The main peaks were ascribed to esseneite ($CaFe_{0.6}Al_{1.3}Si_{1.08}O_6$, PDF#84-1206), featuring ferrous ions; however both 'pure' hedenbergite ($CaFeSi_2O_6$, PDF#87-1704) and iron-doped wollastonite ($Ca_{2.87}Fe_{0.13}Si_3O_9$, PDF#83-2198), featuring ferrous ions, could not be excluded. Hematite (featuring only Fe^{3+} ions, Fe_2O_3, PDF#89-0691) was detected only below 1000 °C, whereas magnetite (Fe_3O_4, PDF#89-0691) was found at all temperatures.

The precipitation of rigid crystal inclusions in softened glass generally determines a dramatic increase of viscosity; in foams, this has fundamental consequences on the ratio between open and closed porosity. As previously observed, the reshaping of porosity in alkali-activated soda-lime glass foams, not particularly prone to crystallization, favoured the formation of closed cells (Rincón et al., 2017). On the contrary, in a glass sensitive to crystallization, the open-celled structure obtained after low temperature foaming could remain practically unaltered (Elsayed et al., 2017).

From the density and porosity data reported in Table 2 we can say that the ratio open/closed porosity, in our system, could be effectively tuned depending on the balance between crystallization and viscous flow. The higher amounts of closed porosity correspond to the lowest temperature (800 °C), at which crystallization was limited (see Fig.4b), and to the highest temperature (1000 °C), at which the enhanced crystallization could be compensated by reduced viscosity of the residual glass phase. For the intermediate temperature (900 °C), the porosity remained mostly open.

Table 2 reports also data concerning the compressive strength of the developed foams. Given the particular microstructures, the strength values are quite promising. In fact, the compressive strength of foams (σ_c) is generally expressed by the Gibson–Ashby equation (Gibson and Ashby, 1999):

$$\sigma_c = \sigma_{bend}[C\ \varphi\ \rho_{rel}^{3/2} + (1-\varphi)\rho_{rel}] \quad (5)$$

where σ_{bend} is the bending strength of the solid phase, C is a dimensionless constant (being ~0.2), ρ_{rel} is the relative density (ρ_{rel} = 1-P/100, where P is the total porosity) and φ is the material fraction at the cell edges. If we consider the foams fired at 900 °C as mostly open-celled, φ could be assumed to be equal to 1: with the observed compressive strength, the bending strength of the solid phase (σ_{bend}) should be above 110 MPa (for the sample with 30% slag), comparing well with the bending strength of dense glass-ceramics (Rincón et al., 2016). The crystallization was evident from the observation of cell struts, as shown in Fig.5 (detail of solid between adjacent interconnected cells).

Owing to the good strength-to-density ratios, the developed foams could be applied, in buildings, for thermal and acoustic insulation. The open celled structure actually opens the way to further applications, as catalytic supports or filters. Any exploitation, however, would not be possible without assessing the absolute safety of the waste-derived materials. The leaching data reported in Table 3 through the application of the EN 12457-2 leaching test show that, for all the metal ions tested, the samples were well below the thresholds for non-hazardous materials, according to European Norm 2003/33/EC, 2003. Concerning the

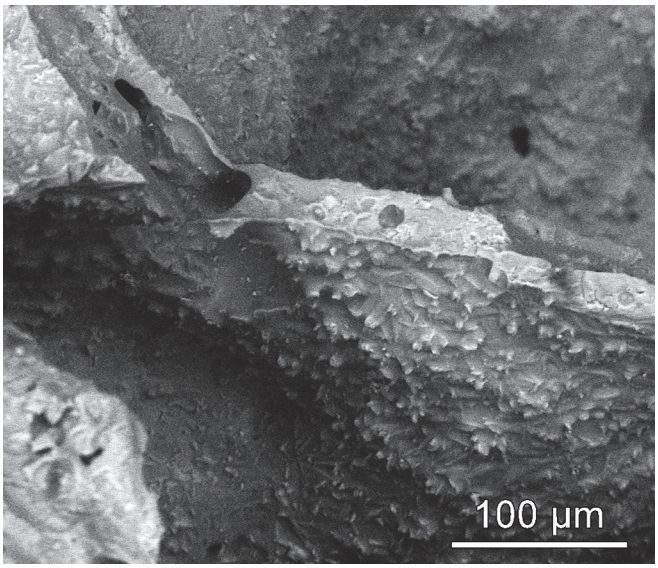

Fig. 5. - High magnification details (SEM) of 80/20 foam fired at 900 °C.

Table 2
Density, porosity and mechanical properties of the developed glass ceramic foams.

Slag %	Firing T (°C)	Density, ρ (g/cm^3)			Porosity (%)			Strength, σ_{comp} (MPa)
		Geometric	Apparent	True	Total	Open	Closed	
20	800	0.55 ± 0.02	1.63 ± 0.08	2.64 ± 0.01	79 ± 4	66 ± 8	12 ± 5	1.6 ± 0.8
	900	0.47 ± 0.02	1.90 ± 0.10	2.63 ± 0.01	82 ± 4	75 ± 9	6 ± 5	1.3 ± 0.1
	1000	0.59 ± 0.02	1.13 ± 0.06	2.75 ± 0.01	78 ± 3	47 ± 8	30 ± 5	2.2 ± 0.4
30	800	0.62 ± 0.02	1.57 ± 0.02	2.67 ± 0.01	76 ± 4	60 ± 4	16 ± 2	4.3 ± 0.9
	900	0.59 ± 0.02	1.99 ± 0.01	2.71 ± 0.01	78 ± 3	70 ± 4	8 ± 1	2.3 ± 0.4
	1000	0.69 ± 0.05	1.33 ± 0.03	2.83 ± 0.01	72 ± 7	48 ± 9	27 ± 2	3.3 ± 0.9

Table 3
Results from leaching tests.

Element (ppm)	SLG/CS 80/20		SLG/CS 70/30		Limits [2003/33/EC, 2003] (ppm)	
	800 °C	900 °C	800 °C	900 °C	Inert material	Non-hazardous material
As	0.0180	<0.0225	<0.0205	<0.0016	0.5	2
Ba	0.0148	<0.0141	<0.0160	0.0044	20	100
Cd	<0.0002	<0.0271	<0.0272	<0.0066	0.04	1
Cr	0.4419	0.2953	0.1104	0.1200	0.5	10
Cu	0.0666	<0.0453	<0.03260	<0.0134	2	50
Mo	0.1177	0.0253	0.0279	0.0351	0.5	10
Ni	0.0018	<0.0443	<0.0439	<0.0237	0.4	10
Pb	0.0293	<0.0100	<0.0101	0.0129	0.5	10
Se	0.0122	<0.0280	<0.0260	<0.0045	0.1	0.5
Zn	0.1694	<0.0612	<0.0642	<0.0195	4	50
Final pH	9.46	9.73	9.26	9.58		

thresholds for inert materials, only the 80/20 sample treated at 800 °C had molybdenum ions above the limit. The findings are particularly significant since, given the high specific area of porous materials, the leaching test was extremely severe. The simple sintering with soda-lime glass is confirmed to be a valid waste stabilization method (Bontempi et al., 2010; Ponsot et al., 2015).

A final observation concerns further applications for the best samples (fired 900 °C, showing both good mechanical properties and chemical resistance), according to the presence of magnetite, in turn leading to a ferri-magnetic behaviour. Ferri-magnetic materials, in fact, may dissipate electromagnetic energy upon magnetization hysteresis (Ponsot et al., 2014; Rincón et al., 2016). With a TEM field within a coaxial waveguide, for frequencies from 0.1 MHz up to 3 GHz, the 80/20 sample has shown a not negligible value of shielding effectiveness (SE) in the 2–2.6 GHz range, with a marked peak (about 7 dB) near 2.4 GHz, as reported in Fig. 6. Oscillations in the data (of about 1 dB), already shown in past experiments (Maschio et al., 2016), are probably due to the particular test set-up.

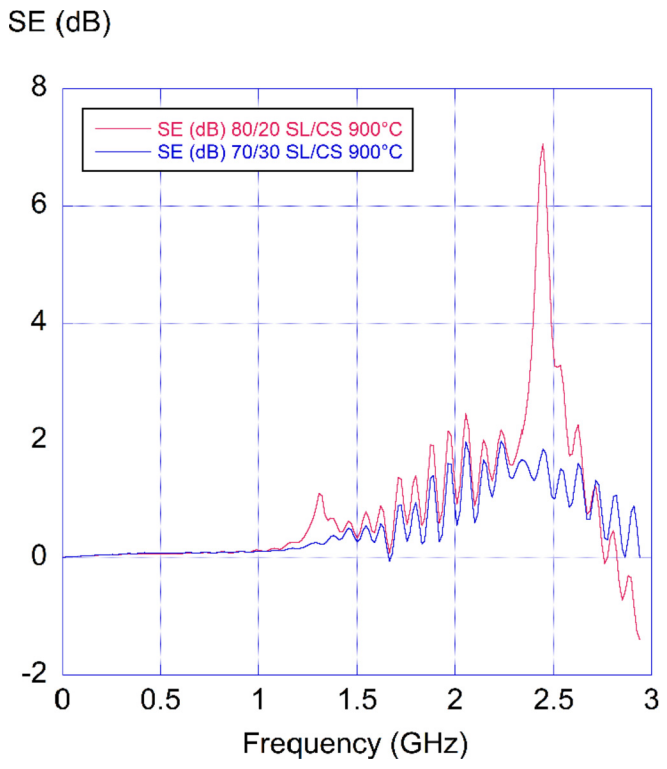

Fig. 6. Shielding effectiveness (SE) of two test samples (about 6 mm thick) with different slag content (80/20 and 70/30) in the range from 0.1 MHz to 3 GHz.

The shielding effect needs additional tests for clarifying the difference between samples with different slag content, and it will be object of future investigations. In any case, these preliminary results are encouraging for the development of low-cost, waste-derived electromagnetic shields alternative to those already reported, depending on specific additives (e.g. carbon fibres in cement based composites) (Zornoza et al., 2010). We can envisage the development of 'multifunctional' lightweight glass-ceramic panels, coupling good thermal and acoustic insulation (associated with the high porosity) with electromagnetic shielding.

4. Conclusions

We may conclude that:

- A novel technique for the development of glass foams from alkali activation of glass suspensions/mechanical foaming/sintering was successfully transferred to mixture of glass and fayalite slag from copper metallurgy;
- The introduction of slag determined a 'dilution' of the calcium silicate hydrated compounds, responsible for low temperature hardening of glass/slag suspensions and attributable to alkaline attack of the soda lime glass fraction; coarser pores could be observed with increasing slag content;
- The sintering at 800–1000 °C led to a substantial 'reshaping' of pores, already available from the mechanical stirring of partially hardened glass/slag suspensions, mainly due to transformations of the slag from copper processing, in turn implying the precipitation of iron oxides, in form of hematite and magnetite; transitions in the valence state of iron ions determined the evolution of oxygen, acting as foaming agent;
- Glass/slag interaction, upon firing, led to the crystallization of Ca–Fe silicates;
- The ratio between open and closed porosity can be tuned depending on the firing temperature and slag concentration; despite a substantial amount of open porosity, the developed glass-ceramics exhibited a remarkable compressive strength;
- Despite the absence of a preliminary melting phase, leading to a homogeneous glass, the direct sintering of glass/slag mixtures led to the stabilization of pollutants from the same slag; the release of heavy metals were particularly limited, even in severe conditions (tests applied to foamed samples, with high specific surface);
- The ferri-magnetic behaviour associated with the presence of magnetite gave additional functionalities to the developed materials; in particular, preliminary tests showed the potential of glass-ceramics in terms of electromagnetic shielding.

Aknowledgements

This project has received funding from the European Union's Horizon 2020 research and innovation programme under the Marie Sklodowska-Curie Innovative Training Network 'CoACH-ETN' ('Advanced glasses, Composites And Ceramics for High growth Industries European Training Network', g.a. no. 642557 - A. Rincón, E. Bernardo) and from the Department of Industrial Engineering of the University of Padova under the Twinning program 'MaVeRIF' ('Materiali Vetroceramici da Rifiuti Industriali per Applicazioni Funzionali' – E. Bernardo, D. Desideri). The authors thank Prof. Yiannis Pontikes (KU Leuven, Belgium) for supplying copper slag and Mr Jacopo Giustozzi (University of Padova) for experimental assistance.

References

Al-Jabri, K.S., Hisada, M., Al-Saidy, A.H., Al-Oraimi, S.K., 2009. Performance of high strength concrete made with copper slag as a fine aggregate. Constr. Build. Mater. 6, 2132–2140.
Attila, Y., Güden, M., Taşdemirci, A., 2013. Foam glass processing using a polishing glass powder residue. Ceram. Int. 5, 5869–5877.
Bontempi, E., Zacco, A., Borgese, L., Gianoncelli, A., Ardesi, R., Depero, L.E., 2010. A new method for municipal solid waste incinerator (MSWI) fly ash inertization, based on colloidal silica. J. Environ. Monit. 11, 2093–2099.
Brinkmann, U., Laqua, W., 1985. Decomposition of fayalite (Fe_2SiO_4) in an oxygen potential gradient at 1,418 K. Phys. Chem. Miner. 5, 283–290.
Chinnam, R.K., Francis, A.A., Will, J., Bernardo, E., Boccaccini, A.R., 2013. Review. Functional glasses and glass-ceramics derived from iron rich waste and combination of industrial residues. J. Non-Cryst. Sol. 365, 63–74.
Cilla, M.S., Colombo, P., Morelli, M.R., 2014. Geopolymer foams by gelcasting. Ceram. Int. 4, 5723–5730.
Cyr, M., Idir, R., Poinot, T., 2012. Properties of inorganic polymer (geopolymer) mortars made of glass cullet. J. Mater. Sci. 6, 2782–2797.
Dussauze, M., Rodriguez, V., Lipovskii, A., Petrov, M., Smith, C., Richardson, K., Cardinal, T., Fargin, E., Kamitsos, E.I., 2010. How does thermal poling affect the structure of soda-lime glass? J. Phys. Chem. C 29, 12754–12759.
Elsayed, H., Rincón Romero, A., Ferroni, L., Gardin, C., Zavan, B., Bernardo, E., 2017. Bioactive glass-ceramic scaffolds from novel 'inorganic gel Casting'and sinter-crystallization. Materials 2, 171.
Gibson, L.J., Ashby, M.F., 1999. Cellular Solids: Structure and Properties. Cambridge university press.
Gorai, B., Jana, R.K., 2003. Characteristics and utilisation of copper slag—a review. Res. Cons. Recycl. 4, 299–313.
Gyurov, S., Rabadjieva, D., Kovacheva, D., Kostova, Y., 2014. Kinetics of copper slag oxidation under nonisothermal conditions. J. Therm. Anal. Calorim. 2, 945–953.
Haq, E.U., Padmanabhan, S.K., Licciulli, A., 2014. In-situ carbonation of alkali activated fly ash geopolymer. Constr. Build. Mater. 781–786.
Hemmings, R.T., Berry, E.E., 1987. On the Glass in Coal Fly Ashes: Recent Advances. MRS Online Proceedings Library Archive.
Iacobescu, R.I., Cappuyns, V., Geens, T., Kriskova, L., Onisei, S., Jones, P.T., Pontikes, Y., 2017. The influence of curing conditions on the mechanical properties and leaching of inorganic polymers made of fayalitic slag. Front. Chem. Sci. Eng. 1–11.
Kambham, K., Sangameswaran, S., Datar, S.R., Kura, B., 2007. Copper slag: optimization of productivity and consumption for cleaner production in dry abrasive blasting. J. Clean. Prod. 5, 465–473.
Lane, M.D., Glotch, T.D., Dyar, M.D., Pieters, C.M., Klima, R., Hiroi, T., Bishop, J.L., Sunshine, J., 2011. Midinfrared spectroscopy of synthetic olivines: thermal emission, specular and diffuse reflectance, and attenuated total reflectance studies of forsterite to fayalite. J. Geophys. Res. Planets E8.
Lottermoser, B.G., 2002. Mobilization of heavy metals from historical smelting slag dumps, North Queensland, Australia. Mineral. Mag. 4, 475–490.
Marangoni, M., Arnout, L., Machiels, L., Pandelaers, L., Bernardo, E., Colombo, P., Pontikes, Y., 2016. Porous, sintered glass-ceramics from inorganic polymers based on fayalite slag. J. Am. Ceram. Soc. 6, 1985–1991.
Maschio, A., Bernardo, E., Desideri, D., Marangoni, M., Ponsot, I., Pontikes, Y., 2016. Shielding effectiveness of construction materials. Int. J. Appl. Electromagn. Mech. 1–2, 137–144.
Martin-Marquez, J., Rincòn, J. Ma., Romero, M., 2008. Effect of firing temperature on sintering of porcelain stoneware tiles. Ceram. Int. 34, 1867–1873.
Mithun, B.M., Narasimhan, M.C., 2016. Performance of alkali activated slag concrete mixes incorporating copper slag as fine aggregate. J. Clean. Prod. 837–844.
Moura, W.A., Gonalves, J.P., Lima, M.B.L., 2007. Copper slag waste as a supplementary cementing material to concrete. J. Mater. Sci. 7, 2226.
Najimi, M., Sobhani, J., Pourkhorshidi, A.R., 2011. Durability of copper slag contained concrete exposed to sulfate attack. Constr. Build. Mater. 4, 1895–1905.
Nazer, A., Pay, J., Borrachero, M.V., Monz, J., 2016. Use of ancient copper slags in Portland cement and alkali activated cement matrices. J. Environ. Manage 115–123.
Onisei, S., Lesage, K., Blanpain, B., Pontikes, Y., 2015. Early age microstructural transformations of an inorganic polymer made of fayalite slag. J. Am. Ceram. Soc. 7, 2269–2277.
Peys, A., Arnout, L., Blanpain, B., Rahier, H., Van Acker, K., Pontikes, Y., 2017. Mix-design parameters and real-life considerations in the pursuit of lower environmental Impact inorganic polymers. Waste Biomass Valorization 1–11.
Ponsot, I., Bernardo, E., 2013. Self glazed glass ceramic foams from metallurgical slag and recycled glass. J. Clean. Prod. 245–250.
Ponsot, I., Pontikes, Y., Baldi, G., Chinnam, R.K., Detsch, R., Boccaccini, A.R., Bernardo, E., 2014. Magnetic glass ceramics by sintering of borosilicate glass and inorganic waste. Materials 7, 5565–5580.
Ponsot, I., Bernardo, E., Bontempi, E., Depero, L., Detsch, R., Chinnam, R.K., Boccaccini, A.R., 2015. Recycling of pre-stabilized municipal waste incinerator fly ash and soda-lime glass into sintered glass-ceramics. J. Clean. Prod. 224–230.
Pontikes, Y., Machiels, L., Onisei, S., Pandelaers, L., Geysen, D., Jones, P.T., Blanpain, B., 2013. Slags with a high Al and Fe content as precursors for inorganic polymers. Appl. Clay. Sci. 93–102.
Provis, J.L., Deventer, Van, Jakob, Jan Stephanus, 2009. Geopolymers: Structures, Processing, Properties and Industrial Applications. Elsevier.
Rawlings, R.D., Wu, J.P., Boccaccini, A.R., 2006. Glass-ceramics: their production from wastes-a review. J. Mater. Sci. 41, 733–761.
Rincón, A., Marangoni, M., Cetin, S., Bernardo, E., 2016. Recycling of inorganic waste in monolithic and cellular glass-based materials for structural and functional applications. J. Chem. Tech. Biotech. 91, 1946–1961.
Rincón, A., Giacomello, G., Pasetto, M., Bernardo, E., 2017. Novel 'inorganic gel casting'process for the manufacturing of glass foams. J. Eur. Ceram. Soc. 5, 2227–2234.
Scarinci, G., Brusatin, G., Bernardo, E., 2005. Glass foams. In: Scheffler, M., Colombo, P. (Eds.), Cellular Ceramics: Structure, Manufacturing, Properties and Applications. WILEY-VCH Verlag GmbH & Co. KGaA, Weinheim, pp. 158–176.
Tchakout, H.K., Rscher, C.H., Kong, S., Kamseu, E., Leonelli, C., 2017. Thermal behavior of metakaolin-based geopolymer cements using sodium waterglass from rice husk ash and waste glass as alternative activators. Waste Biomass Valor 3, 573–584.
Van der Sloot, H.A., Dijkstra, J.J., 2004. Development of horizontally standardized leaching tests for construction materials: a material based or release based approach? Identical leaching mechanisms for different materials. Report No-.ECN-C-04–060 Energy Res. Cent. Neth. 44 (annexes).
Zain, M.F.M., Islam, M.N., Radin, S.S., Yap, S.G., 2004. Cement-based solidification for the safe disposal of blasted copper slag. Cem. Conc. Comp. 7, 845–851.
Zornoza, E., Catalá, G., Jiménez, F., Andión, L.G., Garcés, P., 2010. Electromagnetic interference shielding with Portland cement paste containing carbon materials and processed fly ash. Materiales de Construcción 60, 21–32.